# q-BWF functions to deconvolute the attenuated total reflectance infrared spectra of the barite-group minerals

# q-BWF functions to deconvolute the attenuated total reflectance infrared spectra of the barite-group minerals

**Amelia Carolina Sparavigna**

Department of Applied Science and Technology, Polytechnic University of Turin, Italy

**Abstract:** Here we consider the minerals in the barite group and their attenuated total reflectance (ATR) infrared spectra, that we can find in the RRUFF database. We apply the q-BWF functions to deconvolute the components of the spectra. The q-BWF functions are the asymmetric line shapes that Sparavigna defined in 2023, to generalize the BWF (Breit-Wigner-Fano) functions. Good results are obtained for the deconvolution of barite, celestine and anhydrite ATR-IR spectra.

**Keywords**: Infrared spectroscopy, ATR spectroscopy, q-Gaussian functions, q-BWF functions.

**Introduction -** In 2023 we proposed to perform the fitting of Raman spectra with q-Gaussian line shapes, which are a generalization of the Lorentzian profile. The q-Gaussian is a function based on the Tsallis q-form of the exponential function (Tsallis, 1988). This generalized form of exponential is characterized by a q-parameter. When q is equal to 2, we have the Lorentzian function. If q is close to 1, we have a Gaussian function. For values of q between 1 and 2, we have a bell-shaped symmetric function with power-law wings ranging from Gaussian to Lorentzian tails. As shown on many occasions, the q-Gaussians are suitable for fitting Raman spectra (from examples proposed in SSRN to the SERS cases). However, we can define also an asymmetric function, turning the Breit-Wigner-Fano into a q-BWF function (Sparavigna, 2023). Let us write the BWF as follow:

$$\mathrm{BWF}(x) = C\frac{\left[1-\xi\gamma^{1/2}(x-x_o)\right]^2}{[1+\gamma(x-x_o)^2]}$$

In the function given above, $x_o$ represents the center of the line. When asymmetry parameter $\xi$ is zero, BWF becomes a symmetric Lorentzian function. Note that the center of the line does not correspond to the position of the peak of the function (Ferrari & Robertson, 2000). As in Sparavigna, 2023, we can define the q-BWF function:

$$\text{q-BWF} = C\left[1-\xi\gamma^{1/2}(q-1)^{1/2}(x-x_o)\right]^2[1+(q-1)\gamma(x-x_o)^2]^{1/(1-q)}$$

In fact, the Lorentzian function is substituted by a q-Gaussian function (see Appendix).

We have already applied the q-BWF functions in several occasions (link1, link2, and references therein) for Raman bands. Here we consider the q-BWFs applied to the deconvolution of ATR infrared spectra (Attenuated Total Reflectance) of the barite-group minerals. Let us note that the "reflectance techniques may be used for samples that are difficult to analyze by the conventional transmittance method" (Khoshhesab, 2012). The ATR spectra here analyzed are given by the RRUFF database (Lafuente, 2015). RRUFF database is useful for testing new approaches to the deconvolution of spectra by means of functions which are not included among the line shapes commonly available in curve fitting software (that is, Gaussian, Lorentzian, Voigt, pseudo-Voigt functions). As we will show in our final discussion, asymmetric functions are necessary to represent the ATR spectral bands: the asymmetric q-BWF functions are suitable for purpose.

**Barite-group minerals and their uses -** "Baryte, or barite, ($BaSO_4$) is a mineral consisting of barium sulfate. The baryte group consists of baryte, celestine, anglesite and anhydrite. Baryte and celestine form a solid

solution (Ba,Sr)$SO_4$" (Strekeisen, 2020). In Wikipedia, it is told that worldwide, baryte "is used as a weighting agent for drilling fluids in oil and gas exploration to suppress high formation pressures and prevent blowouts". Details are given by Bonel, 2005. In fact, the countries where "continuous massive drilling in oil and gas fields" are present, are always requiring high quality barite for drilling fluids (Oahimire et al., 2021, Afolayan et al., 2021) and are searching for new ores. The finding of new high-grade mineral ores is relevant to prevent any crisis of barite supply-chain. In general, the "global dependence on a limited number of countries for specific mineral commodities could lead to sudden supply disruptions" for some countries (Bleiwas and Miller, 2015, referring to USA case), and barite is one of these commodities.

Studies regarding the drilling fluids have a high relevance to oil and gas extraction. A comprehensive review about the nanoparticle-based drilling fluids is proposed by Medhi et al., 2024. The "effect of nanoparticles with different compositions and sizes on the rheological properties, filtration losses, and lubricating ability of drilling fluids has been experimentally studied" by Minakov, et al., 2018. For example, "the addition of silica to a clay-based fluid containing barite particles" influences the plastic viscosity and shear yield stress (Minakov et al., 2015, mentioning Salih et al., 2016). The use of surfactant-inhibited nanoparticles of barite has been also considered (Whyte, 2019).

Another relevant barite application is its use for shielding materials. Kinnunen et al., 2024, propose the baryte tailings for radiation shielding in nuclear waste disposal. Moreover, as told by Kinnunen and coworkers, baryte is "used in drilling mud, medical industry, glass making, paint and rubber industry, industrial chemicals, and in other applications, such as plastics," and it is listed as critical raw material for European Union. In PubChem too, about the barium sulfate, we find that it is "used in various manufacturing applications and mixed into heavy concrete to serve as a radiation shield. This drug is used as a contrast agent in diagnostic x-ray procedures. Therapeutic advantages of barium sulfate in diagnostic procedures include both its low water solubility and high level of clearance from the body". In Budi et al., 2019, we can find studied the "attenuation coefficient of barite concrete subjected to gamma-ray radiation". The "use of barite concrete for radiation shielding against gamma-rays and neutron" has been investigated by Daungwilailuk et al., 2022. In general, studies about the heavyweight barite concrete have been given by Topçu, 2003, Saidani et al., 2014, Binici, 2010. For what is regarding glasses, studies have been also dedicated to the production of ancient Chinese glasses (Ma et al., 2021, Qin et al., 2016).

Celestine $Sr(SO_4)$ "and the carbonate mineral strontianite are the principal sources of the element strontium, commonly used in fireworks and in various metal alloys" (Wikipedia). Alishahi et al., 2023, have studied the "optimization of the strontium compounds production, using a celestine ore sample". Celestine and blue dust have been used for the preparation of strontium hexaferrite powder by Tiwary et al., 2008. By means of first-principles calculations, Hu and coworkers, 2013, have studied "the crystal structure, energy band structure, density of states, optical properties, and bonding properties of celestine".

Anglesite $Pb(SO_4)$ has uses in: batteries, ammunition, radiation, plumbing, sound absorber, shield of x-rays, paint pigment, glass and insecticides (Vedantu). Anhydrite $Ca(SO_4)$ "can be substituted for gypsum in some of its uses. Both minerals are crushed for use as a soil treatment, and in this purpose anhydrite is superior. … Small amounts of anhydrite are used as drying agents in plaster, paint, and varnish. It is also used along with gypsum to produce plaster, joint compound, wallboard, and other products for the construction industry" (chemicalbook). About anhydrite, let us note that in Huang et al., 2020, we can find reported that the mineral is produced from gypsum by microorganisms of the Atacama Desert, Chile. Microorganisms extract water from gypsum rocks, enabling their colonies "to sustain life in this extreme environment". The extracted water is the gypsum crystallization water. Microorganisms are "inducing a phase transformation from gypsum ($CaSO_4 \cdot 2H_2O$) to anhydrite ($CaSO_4$)". In Huang et al., it is told that "Interestingly, anhydrite was observed in areas populated with microorganisms, while substrate areas without microorganisms consisted only of gypsum. Fourier transform-infrared spectroscopy (FTIR) maps were acquired in the areas with microorganisms to further verify the existence of anhydrite phase" (Huang et al., mentioning Bishop et al., 2014, Liu et al., 2009). About microbial communities in the Atacama Desert, see Crits-Christoph et al., 2013.

**RRUFF barite -** The deconvolutions in the following figures are obtained by means of software Fityk (Wojdyr, 2010), after defining in it the q-Gaussian and q-BWF functions (see Appendix for further details). The infrared spectra are given in RRUFF through the attenuated total reflectance technique. The instrumental settings are according SensIR Durascope on a Nicolet Magna 860 FTIR.

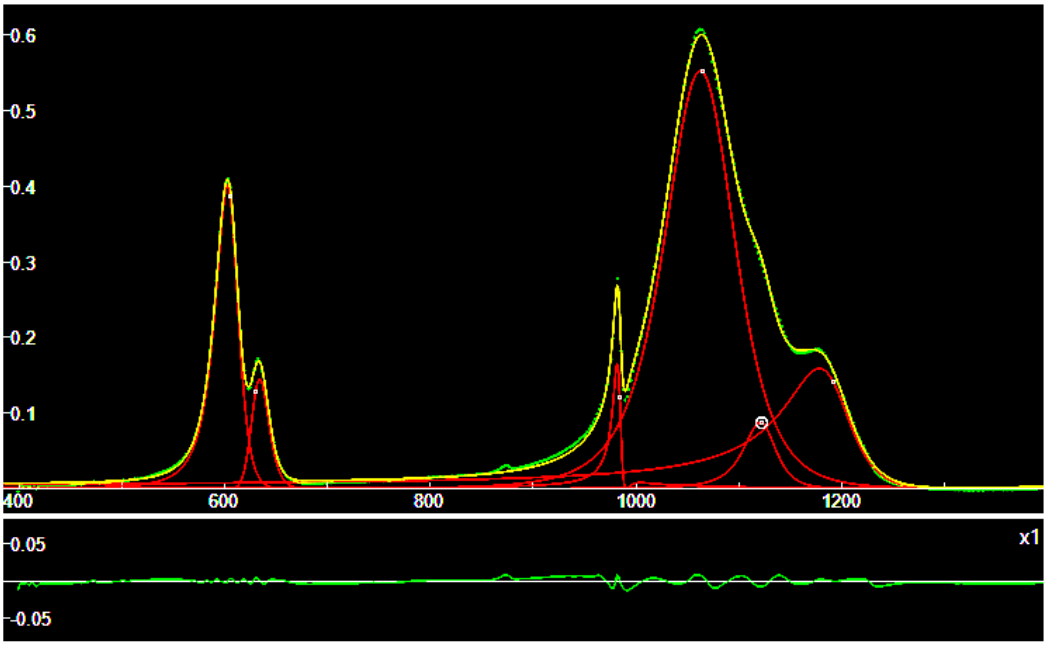


*Fig.1: Deconvolution of baryte RRUFF R040036 ATR spectrum. We use q-BWF functions (in red). The lower part of the images is showing the misfit, that is the difference between data (green) and the sum of components (yellow curve). Note that the position of the center of a q-BWF function, the white dot, is different from the position of the peak.*

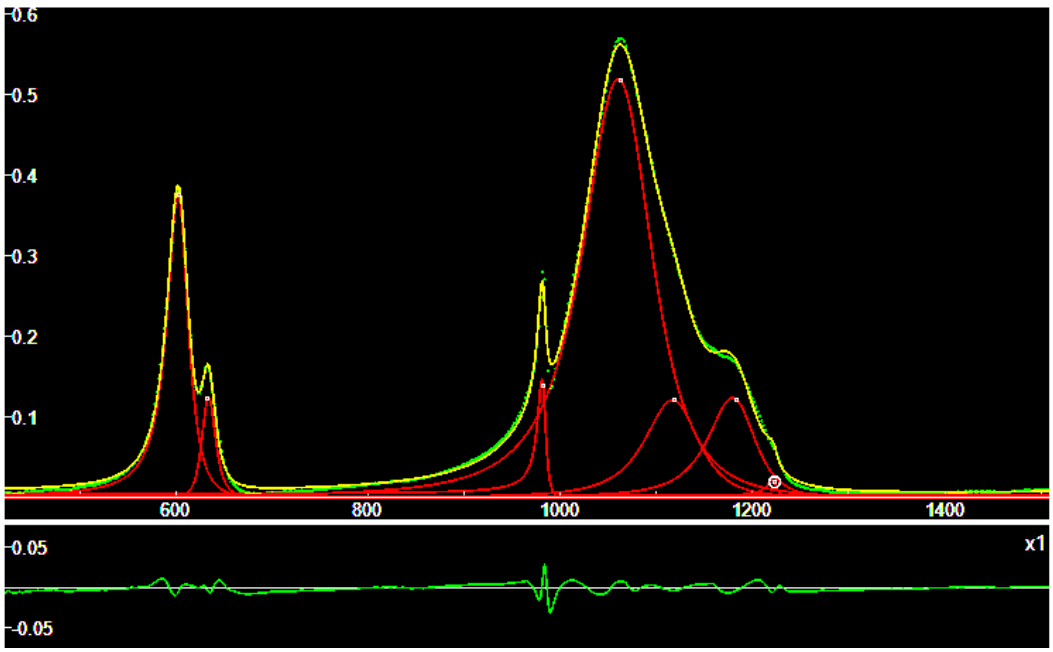


*Fig.2: Deconvolution of baryte RRUFF R050335 ATR spectrum.*

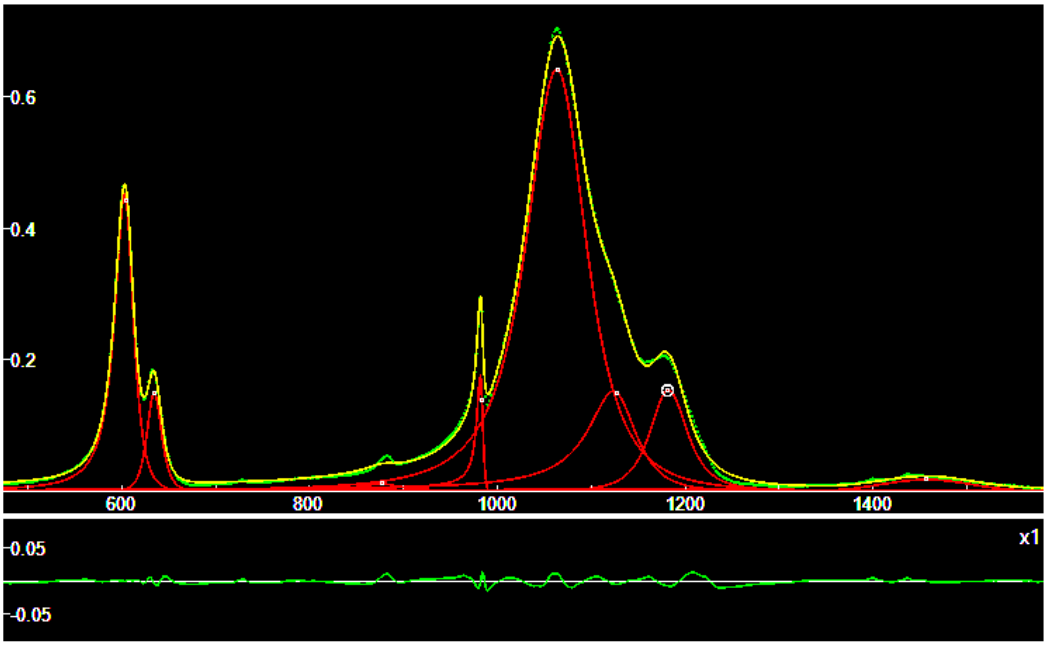


*Fig.3: Deconvolution of baryte RRUFF R050342 ATR spectrum.*

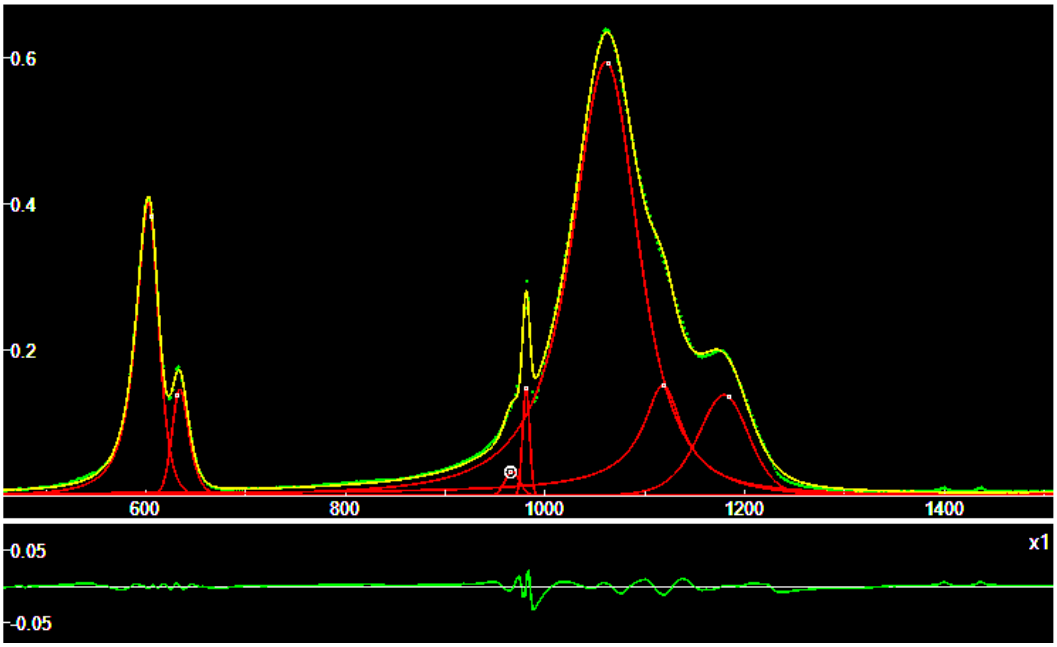


*Fig.4: Deconvolution of baryte RRUFF R050375 ATR spectrum.*

**Results -** In the NIST Chemistry WebBook, we can find the barite infrared spectrum. We can use the transmittance /absorbance, to determine the peaks. The peaks are at ($cm^{-1}$): 615, 654, 987, 1077, 1128 and 1192. From the figures given above, we find (position of the peaks of the components, in $cm^{-1}$):

| | | | | | | | |
|---|---|---|---|---|---|---|---|
| R040036 | 602 | 634 | | 981 | 1062 | 1122 | 1180 |
| R050335 | 602 | 634 | | 981 | 1061 | 1120 | 1180 |
| R050342 | 602 | 634 | | 982 | 1063 | 1126 | 1181 |
| R050375 | 602 | 634 | 967 | 981 | 1060 | 1119 | 1180 |
| NIST | 615 | 654 | | 987 | 1077 | 1128 | 1192 |

Comparing the positions of q-BWF peaks with the NIST peaks, we can find a shift of the positions.

| | | | | | | | |
|---|---|---|---|---|---|---|---|
| R040036 | 606 | 630 | 984 | | 1065 | 1123 | 1191 |
| R050335 | 604 | 633 | 982 | | 1064 | 1119 | 1183 |
| R050342 | 604 | 634 | 983 | | 1065 | 1127 | 1182 |
| R050375 | 605 | 631 | 981 | 965 | 1063 | 1119 | 1184 |
| NIST | 615 | 654 | 987 | | 1077 | 1128 | 1192 |

Comparing the centers of q-BWF components with the NIST peaks.

**Celestine** – Let us consider also the deconvolution of the IR spectra of the other minerals of the group. Here, in the Figures 5 and 6, the deconvolution of the celestine spectra available from RRUFF database.

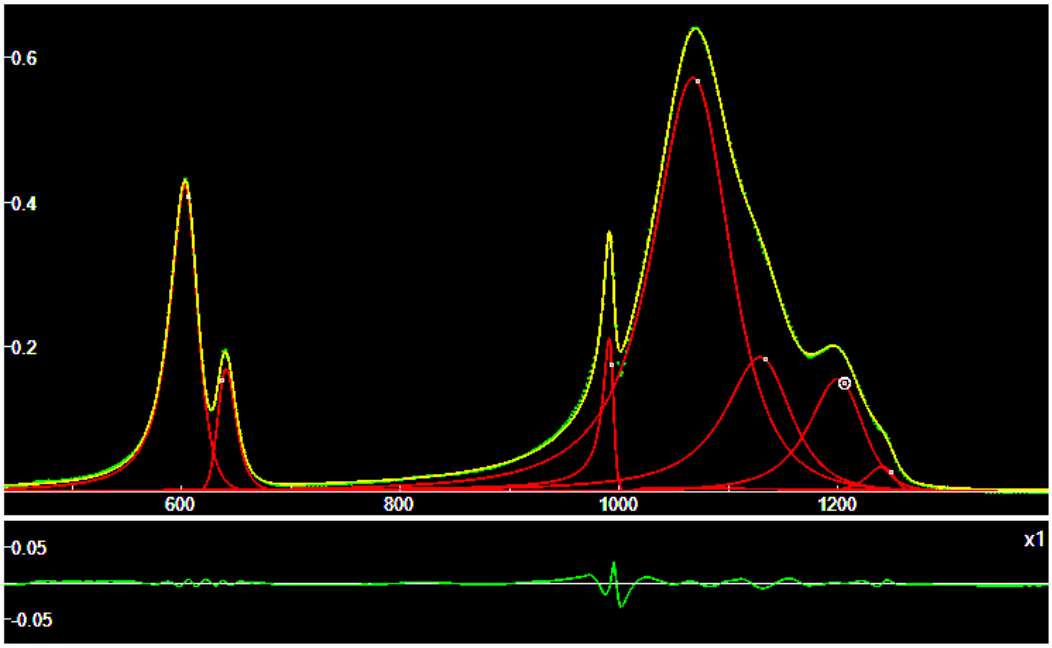


*Fig.5: Deconvolution of celestine RRUFF R040007 ATR spectrum.*

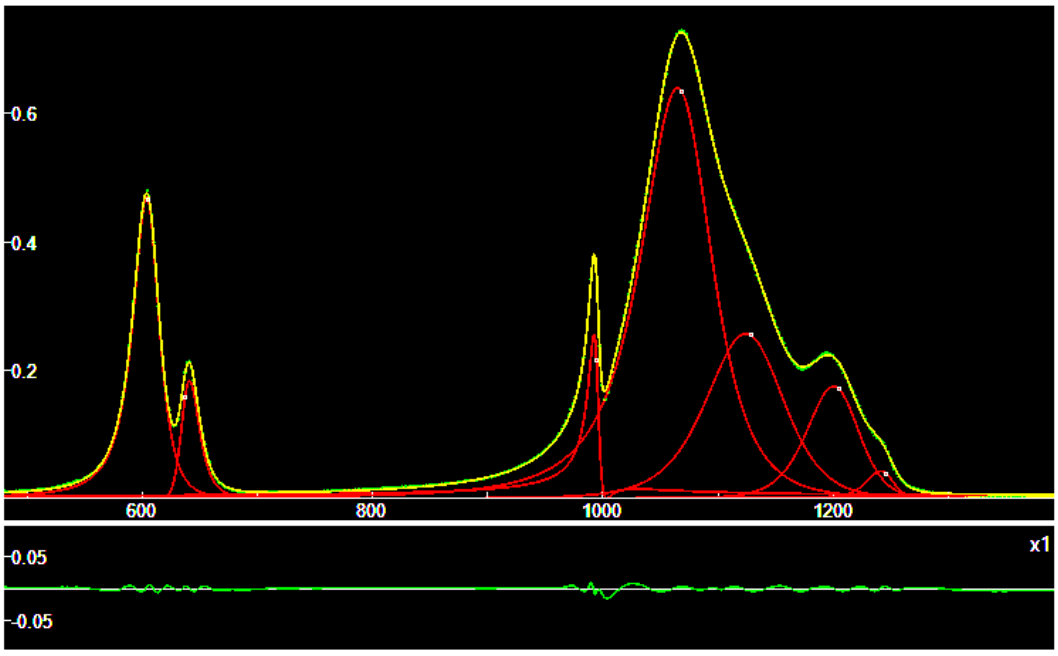


*Fig.6: Deconvolution of celestine RRUFF R050008 ATR spectrum.*

At the web site spec4gem, we can find a celestine IR reflectance spectrum. We can compare the position of the q-BWF peaks (in $cm^{-1}$).

| | | | | | | | |
|---|---|---|---|---|---|---|---|
| R040007 (peaks) | 603 | 640 | | 991 | 1067 | 1130 | 1200 | 1240 |
| R040007 (centers) | 606 | 637 | | 993 | 1072 | 1133 | 1206 | 1248 |
| R050008 (peaks) | 603 | 641 | | 992 | 1063 | 1124 | 1200 | 1244 |
| R050008 (centers) | 605 | 638 | | 995 | 1968 | 1128 | 1206 | 1246 |
| SPEC4GEM | 615 | 643 | 654 | 991 | 1098 | 1148 | 1198 | 1250 |

**Anglesite –** In the following three images, the decomposition of anglesite.

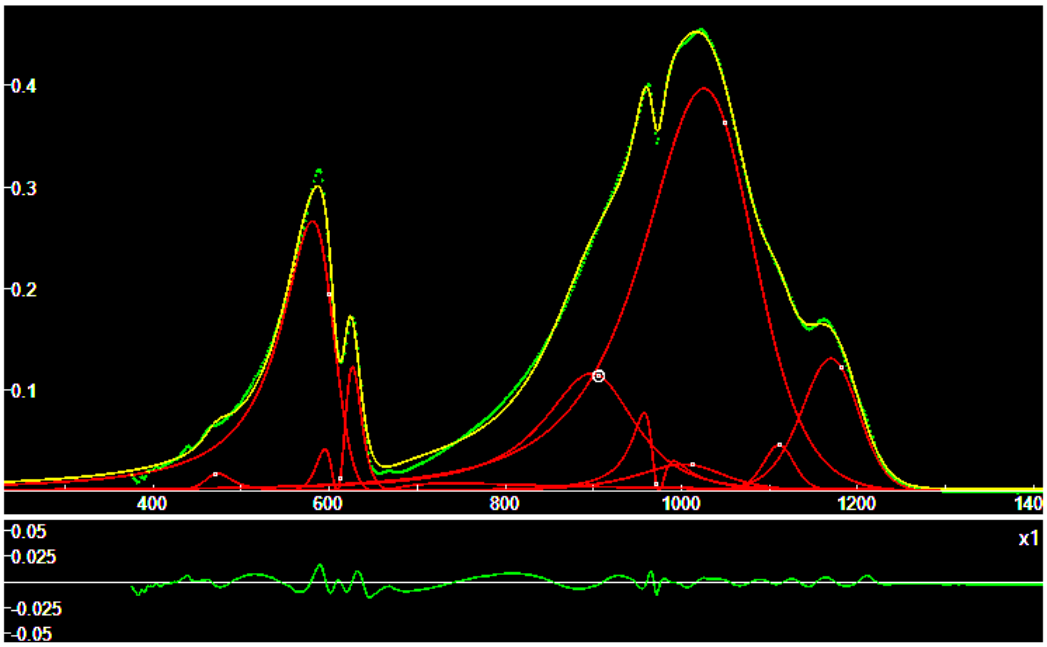


*Fig.7: Deconvolution of anglesite RRUFF R040004 ATR spectrum.*

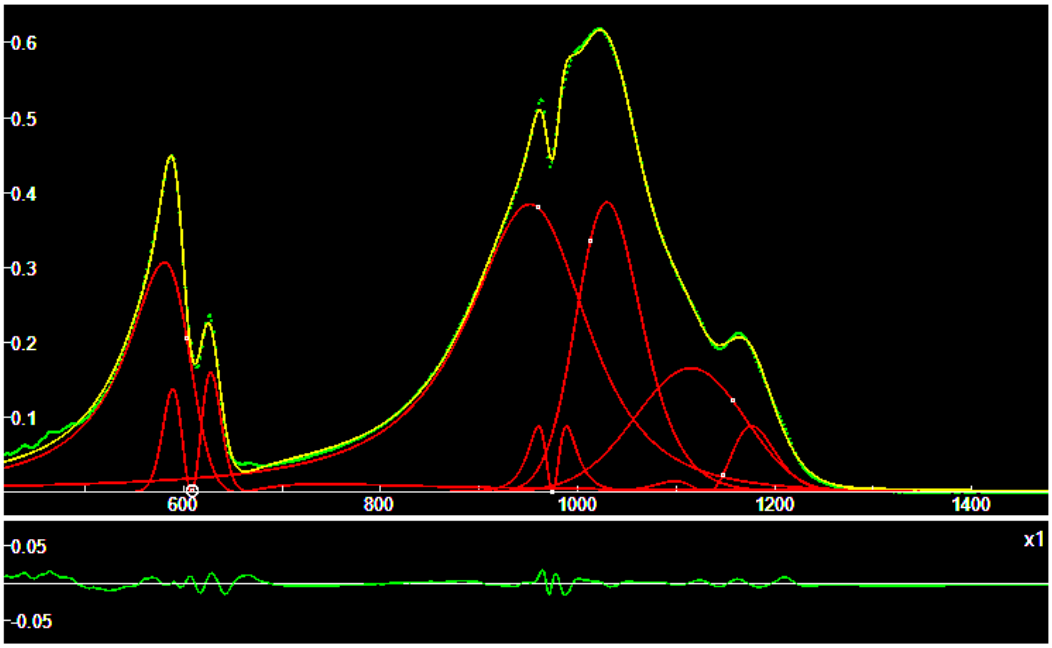


*Fig.8: Deconvolution of anglesite RRUFF R050052 ATR spectrum.*

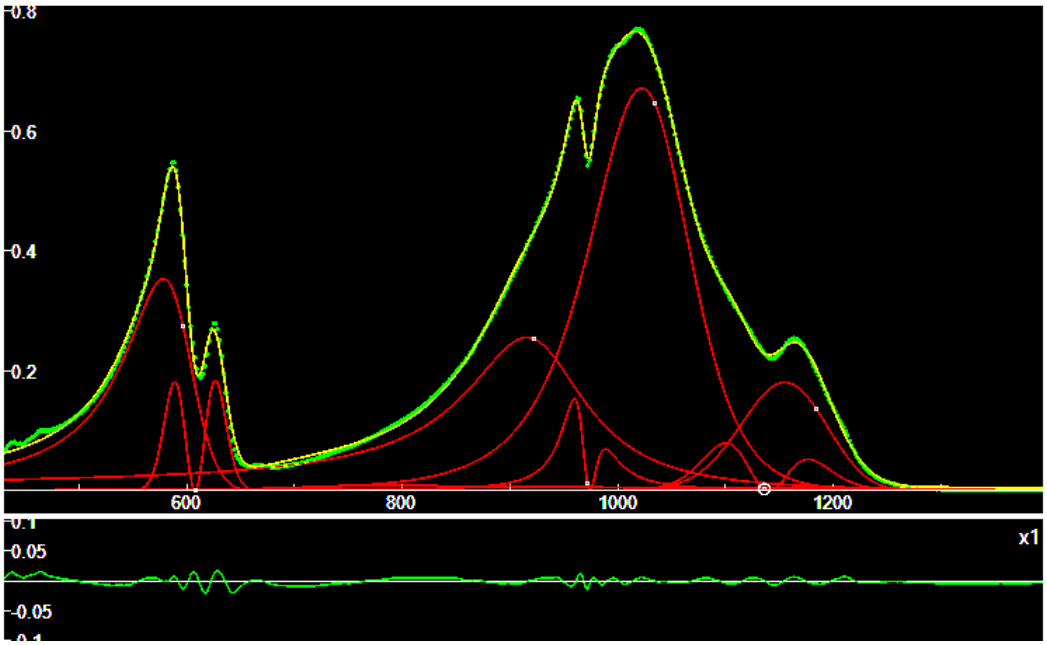


*Fig.9: Deconvolution of anglesite RRUFF R050408 ATR spectrum.*

In Monneron-Gyurits et al. 2022, we can find an infrared characterization of synthetic anglesite. We find evidenced the peaks at 625, 965, 993, 1166 $cm^{-1}$. In the case of R050408, we find: 587, 625, 961, 1016, 1164 $cm^{-1}$.

**Anhydrite** - In RRUFF database we can find two ATR spectra of anhydrite. Let us consider them and compare with data from Prasad et al., 2005.

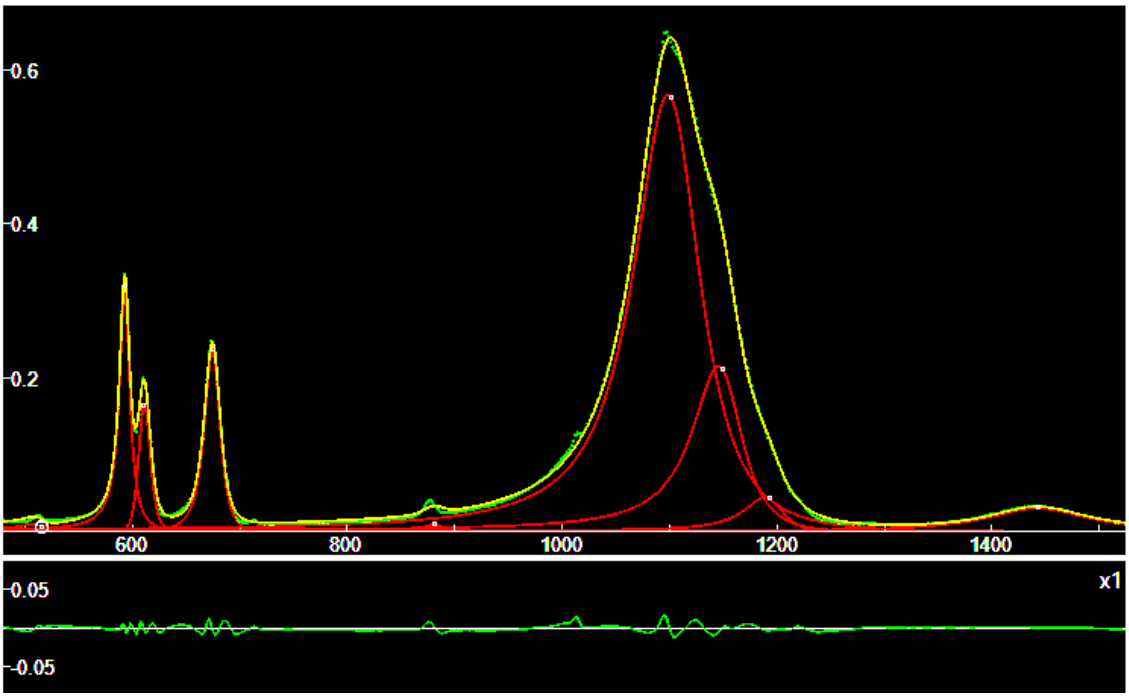


*Fig.10: Deconvolution of anhydrite RRUFF R040012 ATR spectrum.*

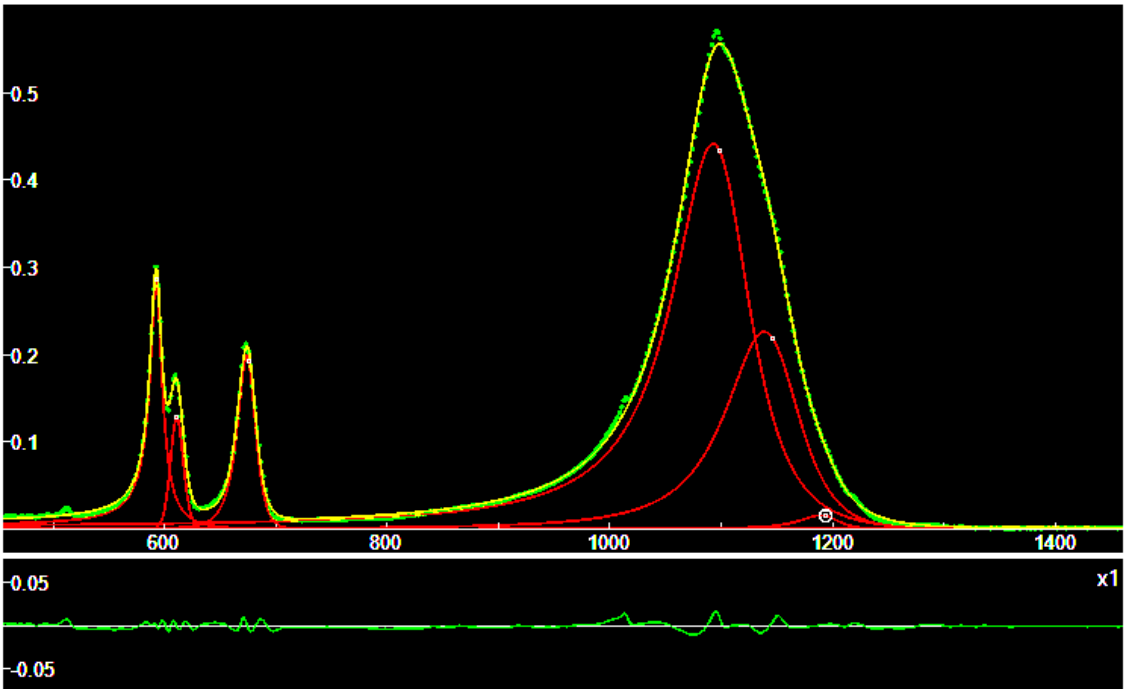


*Fig.11: Deconvolution of anhydrite RRUFF R040061 ATR spectrum.*

Considering the positions of the q-BWF peaks, we can obtain (in $cm^{-1}$) a comparison with Prasad et al., 2005, data:

| | | | | | | | |
|---|---|---|---|---|---|---|---|
| R040012 | 593 | 611 | 674 | 1100 | 1148 | 1191 | 1443 |
| R040061 | 592 | 610 | 678 | 1093 | 1143 | 1193 | |
| Prasad et al., 2005 | 595 | 615 | 676 | 1014 | 1124 | 1157 | |

In the cases of barite, celestine and anhydrite, we have rather simple deconvolutions, which provide an easy comparison with data. The case of anglesite requires further investigation for sure.

**Discussion**

We have considered the ATR spectra from RRUFF database and compared with infrared spectra, available from literature. As told by Subramanian and Rodriguez-Saona, 2009, ATR is "one of the most commonly used sampling techniques in recent times". When an IR light beam passes from a medium with a high refractive index into "a medium of low refractive index (sample)", we can observe that "at a particular angle of incidence, almost all the light waves are reflected back. This phenomenon is called total internal reflection. In this condition, some amount of the light energy escapes the crystal and extends a small distance (0.1–5 μm) beyond the surface in the form of waves". These waves are the evanescent waves. "The intensity of the reflected light reduces at this point. This phenomenon is called *attenuated total reflectance*" (Subramanian & Rodriguez-Saona, 2009).

"The partial penetration of the IR light by an evanescent wave allows an absorption spectrum to be recorded" (see for instance, QD-Europe). The penetration depth of the evanescent wave is a function of the angle of incidence at the sample surface interface. "Deeper penetration into a sample is achieved with either a smaller incident angle or a lower refractive index ATR crystal" (QD-Europe). It is stressed that an ATR spectrum is "different to that obtained for the same sample when collected as a transmission spectrum", since measurement methods are different, being differences dictated "by the fundamental way the sample information is being collected". In transmission spectroscopy, the light passes through the sample, "whereas ATR spectroscopy is the interaction of light by passage into the surface of a sample species. *Note that neither method can be regarded as giving the "correct" spectrum – they are simply different*" (QD-Europe). The web site details the role of wavelength and refractive index on the penetration depth of the light. Also, the differences of intensities,

the band shift, and the band asymmetries that we observe when an ATR spectrum is compared to a transmission spectrum, are discussed. For instance, regarding the band distortion, it is told that "sometimes in ATR measurements the absorption bands can become *slightly asymmetric* compared to the bands seen in transmission measurements" (QD-Europe). The deformation of the band shape is due to "the rapid change of refractive index of the sample across the band". "The refractive index of the sample varies from a low value on the short wavelength side of the band to a high value on the long wavelength side. This causes the effective penetration depth to also rapidly increase toward the long wavelength side and causes the characteristic shape of the bands seen" (D-Europe).

Is it possible to compare the IR spectral results? Let us consider the observations made by Kendix, 2009: "in most cases comparison of standard spectra collected in FIR transmission and FIR ATR mode leads to only a few differences. The most obvious, when comparing transmission with ATR, is the distortion of band shape. The ATR band shape appears *asymmetrical* in the lower wavenumber region when compared to spectra collected in transmission mode. Also, *intensity differences* are noticed. However, the biggest difference can be the *shift* of strong absorbing bands moving to lower wavenumbers in ATR mode" (Kendix, 2009). Usually, "the shifts observed are small, approximately 1-10 $cm^{-1}$, but for very strong absorbing compounds the shifts observed can be as big as 30-50 $cm^{-1}$" (Kendix, 2009). Then the ATR spectra can be "considerably different from transmission spectra with respect to intensities, band shift and band distortions" (Kendix, 2009). If we could use both techniques, we could obtain databases, for instance, to "identifying unknown pigment samples" (Kendix considers pigments in the framework of analyses of cultural heritage materials). "Perhaps it would be less time consuming and more convenient to try to correct the ATR spectrum to simulate a transmission spectrum by using a correction algorithm" (Kendix, 2009). Besides advanced ATR correction algorithms, we could "try applying the Kramers-Kronig transformation on the ATR spectra". However, "the transformation of spectra are usually problematic". Kendix proposes an example of transformations with algorithm and KK relations on cinnabar ATR spectrum, concluding that it is better to collect both transmission and ATR spectra "to build a database for comparison with unknown samples using both techniques as means of detection and identification".

As we have seen, ATR measurement method is producing intrinsically asymmetric bands, and therefore, for the deconvolution of the spectrum, an asymmetric band shape is required. We have shown that, using the asymmetric q-BWF functions, we can determine the components of ATR spectra, useful for comparison with infrared data available from literature. We have obtained good results for barite, celestine and anhydrite. The anglesite case is trickier and requires further investigations.

**Appendix – q-Gaussian and q-BWF functions**

Sparavigna, 2023, proposed for the first time the use of q-Gaussian function in Raman spectroscopy. She defined also the q-BWF functions which are generalizing the Breit-Wigner-Fano (asymmetric) line shape in the framework of the q-exponential function. Here we show how to apply, by means of Fityk software, the q-Gaussian and the q-BWF functions in spectroscopy. Let us remember that the q-Gaussian functions are probability distributions proper of the Tsallis statistics (Tsallis, 1988, Hanel et al., 2009). The q-Gaussian is defined as: $f(x) = Ce_q(-\beta x^2)$, where $e_q(.)$ is the q-exponential function and $C$ a scale constant (in the exponent, $\beta = 1/(2\sigma^2)$). The q-exponential has expression: $e_q(u) = [1 + (1-q)u]^{1/(1-q)}$. Then, the q-Gaussian function with center of the band at $x_o$ is:

$$q\text{-}Gaussian = Cexp_q(-\beta(x-x_o)^2) = C[1 + (q-1)\beta(x-x_o)^2]^{1/(1-q)}$$

The expression of the q-BWF function has been given in the Introduction.

In Fityk, a q-Gaussian function can be defined in the following manner:

define Qgau(height, center, hwhm, q=1.5) = height*(1+(q-1)*((x-center)/hwhm)^2)^(1/(1-q))

q=1.5 the initial guessed value of the q-parameter. Parameter hwhm is the half width at half maximum of the component. When q=2, the q-Gaussian is a Lorentzian function, that we can find defined in Fityk as:

Lorentzian(height, center, hwhm) = height/(1+((x-center)/hwhm)^2)

When q is close to 1, the q-Gaussian becomes a Gaussian function. The q-BWF can be defined as:

Qbreit(height, center, hwhm, q=1.5, xi=0.1) = (1-xi*(q-1)*(x-center)/hwhm)^2*height*(1+(q-1)^0.5 *((x-center)/hwhm)^2)^(1/(1-q))

And the BWF can be defined as:

Breit(height, center, hwhm, xi=0.1 ) = (1-xi*(x-center)/hwhm)^2*height/(1+((x-center)/hwhm)^2)

Using +xi instead of -xi does not change the fitting results in Fityk.

**References**


1. Afolayan, D. O., Adetunji, A. R., Onwualu, A. P., Ogolo, O., & Amankwah, R. K. (2021). Characterization of barite reserves in Nigeria for use as weighting agent in drilling fluid. Journal of Petroleum Exploration and Production Technology, 11(5), 2157-2178.
2. Alishahi, A., Noaparast, M., Ashni, A. R., & Nasab, M. H. (2023). The optimization of the strontium compounds production, using a celestine ore sample. Rudarsko-geološko-naftni zbornik, 38(4), 53-62.
3. Binici, H. (2010). Durability of heavyweight concrete containing barite. International journal of materials research, 101(8), 1052-1059.
4. Bishop, J. L., Lane, M. D., Dyar, M. D., King, S. J., Brown, A. J., & Swayze, G. A. (2014). What lurks in the martian rocks and soil? Investigations of sulfates, phosphates, and perchlorates. Spectral properties of Ca-sulfates: gypsum, bassanite, and anhydrite. American Mineralogist, 99(10), 2105-2115.
5. Bleiwas, D. I., & Miller, M. M. (2015). Barite: a case study of import reliance on an essential material for oil and gas exploration and development drilling (No. 2014-5230). US Geological Survey.
6. Bonel, K.A. 2005. Barytes. British Geological Survey, Natural Environment Research Council, Keyworth, Nottingham, U.K. 1-28 pages.
7. Budi, G. S., Koentjoro, H., Wijaya, J., & Sikomena, E. F. (2019). The attenuation coefficient of barite concrete subjected to gamma-ray radiation. In MATEC Web of Conferences (Vol. 258, p. 05030). EDP Sciences.
8. Crits-Christoph, A., Robinson, C.K., Barnum, T., Fricke, W.F., Davila, A.F., Jedynak, B., McKay, C.P. and DiRuggiero, J., 2013. Colonization patterns of soil microbial communities in the Atacama Desert. Microbiome, 1, pp.1-13.
9. Daungwilailuk, T., Yenchai, C., Rungjaroenkiti, W., Pheinsusom, P., Panwisawas, C., & Pansuk, W. (2022). Use of barite concrete for radiation shielding against gamma-rays and neutrons. Construction and Building Materials, 326, 126838.
10. Ferrari, A. C., & Robertson, J. (2000). Interpretation of Raman spectra of disordered and amorphous carbon. Physical Review B 61: 14095–14107.
11. Hanel, R., Thurner, S., & Tsallis, C. (2009). Limit distributions of scale-invariant probabilistic models of correlated random variables with the q-Gaussian as an explicit example. The European Physical Journal B, 72(2), 263.
12. Hu, Z., Zhang, C., Li, Y., & Ao, B. (2013). First-principles study of structural, electronic, optical and bonding properties of celestine, SrSO4. Solid state communications, 158, 5-8.
13. Huang, W., Ertekin, E., Wang, T., Cruz, L., Dailey, M., DiRuggiero, J., & Kisailus, D. (2020). Mechanism of water extraction from gypsum rock by desert colonizing microorganisms. Proceedings of the National Academy of Sciences, 117(20), 10681-10687.
14. Kendix, E. L. (2009). Trasmission and Reflection (ATR) Far-Infrared Spectroscopy Applied in the Analysis of Cultural Heritage Materials. Ph.D. Thesis, Alma Mater Studiorum Università di Bologna, Bologna, Italy.
15. Kinnunen, P., Pelto, J., Viitanen, P., Olin, M., & Nieminen, M. (2024). Valorisation of baryte tailings for radiation shielding in plastics and nuclear waste disposal. Heliyon, 10(3).

16. Khoshhesab, Z. M. (2012). Reflectance IR spectroscopy. Infrared spectroscopy-Materials science, engineering and technology, 11, 233-244.
17. Lafuente, B., Downs, R. T., Yang, H., & Stone, N. (2015). 1. The power of databases: The RRUFF project. In Highlights in mineralogical crystallography (pp. 1-30). De Gruyter (O).
18. Liu, Y., Wang, A., & Freemen, J. J. (2009, March). Raman, MIR, and NIR spectroscopic study of calcium sulfates: gypsum, bassanite, and anhydrite. In 40th Annual Lunar and Planetary Science Conference (p. 2128).
19. Medhi, S., Chowdhury, S., Dehury, R., Khaklari, G.H., Puzari, S., Bharadwaj, J., Talukdar, P., & Sangwai, J.S. (2024). Comprehensive Review on the Recent Advancements in Nanoparticle-Based Drilling Fluids: Properties, Performance, and Perspectives. Energy & Fuels, 38(15), pp.13455-13513.
20. Ma, Q., Braekmans, D., Shortland, A., & Pollard, A. M. (2021). The Production and composition of chinese lead-barium glass through experimental laboratory replication. Journal of Non-Crystalline Solids, 551, 120409.
21. Minakov, A. V., Mikhienkova, E. I., Zhigarev, V. A., Neverov, A. L., & Rudyak, V. Y. (2018). A study of the influence of nanoparticles on the properties of drilling fluids. Colloid journal, 80, 418-426.
22. Monneron-Gyurits, M., Joussein, E., Courtin-Nomade, A., Grauby, O., Paineau, E., Reguer, S., & Soubrand, M. (2022). A fast one-pot synthesize of crystalline anglesite by hydrothermal synthesis for environmental assessment on pure phase. Environmental Science and Pollution Research, 1-9.
23. Oahimire, D. M., Ukaegbu, V. U., & Ogbonna, J. F. (2021). Assessment of some baryte ores from Northern Cross-River, Nigeria, for oilfield drilling fluid supplement. Journal of Degraded and Mining Lands Management, 9(1), 3015.
24. Oahimire, D. M., Ukaegbu, V. U., & Ogbonna, J. F. (2021). Quality assessment of some baryte ores in Benue state area, Nigeria for oilfield drilling. Journal of Degraded and Mining Lands Management, 8(4), 2861.
25. Prasad, P. S. R., Krishna Chaitanya, V., Shiva Prasad, K., & Narayana Rao, D. (2005). Direct formation of the γ-CaSO4 phase in dehydration process of gypsum: In situ FTIR study. American Mineralogist, 90(4), 672-678.
26. Qin, Y., Wang, Y., Chen, X., Li, H., Xu, Y., & Li, X. (2016). The research of burning ancient Chinese lead-barium glass by using mineral raw materials. Journal of Cultural Heritage, 21, 796-801.
27. Saidani, K., Ajam, L., & Ouezdou, M. B. (2015). Barite powder as sand substitution in concrete: Effect on some mechanical properties. Construction and Building Materials, 95, 287-295.
28. Salih, A. H., Elshehabi, T. A., & Bilgesu, H. I. (2016, September). Impact of nanomaterials on the rheological and filtration properties of water-based drilling fluids. In SPE Eastern regional meeting (pp. SPE-184067). SPE.
29. Sparavigna, A. C. (2023). q-Gaussian Tsallis Line Shapes and Raman Spectral Bands. Int. J. Sciences, 12(3), 27-40.
30. Sparavigna, A. C. (2023). Asymmetric q-Gaussian functions generalizing the Breit-Wigner-Fano functions. Zenodo. https://doi.org/10.5281/zenodo.8356165
31. Sparavigna, A. C. (2024). Molybdenum Disulfide MoS2 and the q-BWF line shapes (Raman Spectroscopy). ChemRxiv. doi:10.26434/chemrxiv-2024-cprs3-v3
32. Sparavigna, A. C. (2024). Barium Titanate BaTiO3 Raman Spectra and their deconvolution with q-BWF functions. ChemRxiv. doi:10.26434/chemrxiv-2024-dchgr
33. Strekeisen, A. (2020). Baryte. https://www.alexstrekeisen.it/english/sedi/baryte.php
34. Subramanian, A., & Rodriguez-Saona, L. (2009). Chapter 7-Fourier Transform Infrared (FTIR) Spectroscopy in Infrared Spectroscopy for Food Quality Analysis and Contro" l, D. Sun, Ed.
35. Tiwary, R. K., Narayan, S. P., & Pandey, O. P. (2008). Preparation of strontium hexaferrite magnets from celestite and blue dust by mechanochemical route. Journal of Mining and Metallurgy, Section B: Metallurgy, 44(1), 91-100.
36. Topçu, İ. B. (2003). Properties of heavyweight concrete produced with barite. Cement and Concrete Research, 33(6), 815-822.

37. Tsallis, C. (1988). Possible generalization of Boltzmann-Gibbs statistics. Journal of statistical physics, 52, 479-487.
38. Whyte, J. M. (2019, March). Surfactant-Inhibited Barium Sulphate Nanoparticles for Use in Drilling or Completion Fluids. In SPE International Conference on Oilfield Chemistry? (p. D011S001R001). SPE.
39. Wojdyr, M. (2010). Fityk: a general-purpose peak fitting program. Journal of applied crystallography, 43(5), 1126-1128.